J|A|C|S
ARTICLES
Published on Web 04/30/2004

The Effects of Axial Ligands on Electron Distribution and Spin States in Iron Complexes of Octaethyloxophlorin, Intermediates in Heme Degradation

Sankar Prasad Rath, Marilyn M. Olmstead, and Alan L. Balch*

Contribution from the Department of Chemistry, University of California, Davis, California 95616

Received December 9, 2003; E-mail: albalch@ucdavis.edu

Abstract: The results presented here show that the nature of the axial ligand can alter the distribution of electrons between the metal and the porphyrin in complexes where there is an oxygen atom replacing one of the meso protons. The complexes $(1\text{-MeIm})_2Fe^{III}(OEPO)$ and $(2,6\text{-xylylNC})_2Fe^{II}(OEPO^{\bullet})$ (where OEPO is the trianionic octaethyloxophlorin ligand and $OEPO^{\bullet}$ is the dianionic octaethyloxophlorin radical) were prepared by addition of an excess of the appropriate axial ligand to a slurry of $\{Fe^{III}(OEPO)\}_2$ in chloroform under anaerobic conditions. The magnetic moment of $(2,6\text{-xylylNC})_2Fe^{II}(OEPO^{\bullet})$ is temperature invariant and consistent with a simple $S = {}^1/_2$ ground state. This complex with an EPR resonance at $g = 2.004$ may be considered as a model for the free-radical like EPR signal seen when the meso-hydroxylated heme/heme oxygenase complex is treated with carbon monoxide. In contrast, the magnetic moment of $(1\text{-MeIm})_2Fe^{III}(OEPO)$ drops with temperature and indicates a spin-state change from an $S = {}^5/_2$ or an admixed $S = {}^3/_2, {}^5/_2$ state at high temperatures (near room temperature) to an $S = {}^1/_2$ state at temperatures below 100 K. X-ray diffraction studies show that each complex crystallizes in centrosymmetric form with the expected six-coordinate geometry. The structure of $(1\text{-MeIm})_2Fe^{III}(OEPO)$ has been determined at 90, 129, and 296 K and shows a gradual and selective lengthening of the Fe−N(axial bond). This behavior is consistent with population of a higher spin state at elevated temperatures.

Introduction

The six-coordinate complex, $\{(py)_2Fe(OEPO)\}$, shown in Scheme 1 (with L = py) is a widely studied model for the product of heme hydroxylation,[1] the initial step in heme degradation shown in Scheme 2 by either the coupled oxidation process or heme catabolism as mediated by heme oxygenase. Coupled oxidation uses dioxygen and a sacrificial reducing agent, which can be ascorbic acid or hydrazine, to convert heme or a heme protein into oxygenated products, usually verdoheme and an iron complex of biliverdin.[2−4] Heme oxygenase is a non-heme protein that binds heme as substrate and then converts it into biliverdin, free iron ion, and carbon monoxide.[5]

Understanding the electronic structure of $\{(py)_2Fe(OEPO)\}$ has been a complex problem. As seen in Scheme 1, three different resonance structures can be drawn which differ in the way electrons are apportioned between the metal and the ligand. Thus, $L_2Fe^{III}(OEPO)$ contains Fe(III) and a trianionic oxophlorin ligand, while $L_2Fe^{II}(OEPO^{\bullet})$ contains Fe(II) and a dianionic ligand which itself houses an unpaired electron in a π-orbital. Finally, $L_2Fe^{I}(OEPOx)$ is a complex of the unusual Fe(I) oxidation state and contains an oxidized, monoanionic form of the ligand. In addition to the issue of electron distribution, there is also the question of the spin state of the iron. Finally, the oxygen atom represents a peripheral site that is potentially protonated or protonatable.

Scheme 1

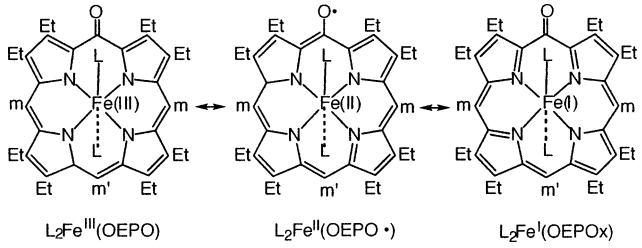

Three routes are available for the formation of $\{(py)_2Fe(OEPO)\}$. It was originally obtained by anaerobic hydrolysis of α-(meso-benzyloxy)heme in pyridine solution.[6] Cleavage of the dimer $\{Fe(OEPO)\}_2$ (see Scheme 3) by simple dissolution in pyridine under the exclusion of dioxygen offers a convenient

(1) Balch, A. L. *Coord. Chem. Rev.* **2000**, *200*−*202*, 349.
(2) Balch, A. L.; Latos-Grażyński, L.; Noll, B. C.; Olmstead, M. M.; Szterenberg, L.; Safari, N. *J. Am. Chem. Soc*. **1993**, *115*, 1422.
(3) Balch, A. L.; Latos-Grażyński, L.; Noll, B. C.; Olmstead, M. M.; Safari, N. *J. Am. Chem. Soc*. **1993**, *115*, 9056.
(4) Hildebrand, D. P.; Tang, H.; Luo, Y.; Hunter, C. L.; Smith, M.; Brayer, G. D.; Mauk, A. G. *J. Am. Chem. Soc.* **1996**, *118*, 12909.
(5) Ortiz de Montellano, P. R. *Acc. Chem. Res*. **1998**, *31*, 543. Maines, M. D. *Heme Oxygenase: Clinical Applications and Functions*; CRC Press: Boca Raton, FL, 1992.
(6) Sano, S.; Sano, T.; Morishima, I.; Shiro, Y.; Maeda, Y. *Proc. Natl. Acad. Sci. U.S.A.* **1986**, *83*, 531.
(7) Balch, A. L.; Noll, B. C.; Reid, S. M.; Zovinka, E. P. *Inorg. Chem.* **1993**, *32*, 2610.

Scheme 2

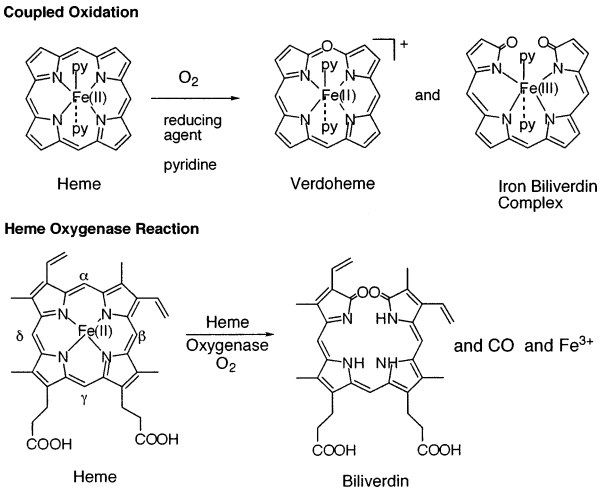

means of preparing this complex.[7] Finally, treatment of $(py)_2Fe^{II}$-(OEP) with hydrogen peroxide in pyridine under the strict exclusion of dioxygen also forms $\{(py)_2Fe(OEPO)\}$.[8]

Air-sensitive $\{(py)_2Fe(OEPO)\}$ has been isolated in crystalline form.[9] The X-ray crystal structure obtained at 143 K reveals a centrosymmetric, six-coordinate complex. The porphyrin core is planar, and, as a result of the centrosymmetric nature of the complex, the pyridine ligands are parallel to one another and lie 13.3° away from the neighboring Fe−N bond. The C−O bond length, 1.289(4) Å, is consistent with the presence of keto group, and there is no other evidence for protonation of the oxygen atom. The Fe−N bond lengths reveal that the in-plane Fe−N distances (2.055(2) and 2.051(2) Å) are shorter than the out-of-plane Fe−N distance (2.265(2) Å). These distances indicate that the iron is in a high-spin state in the crystalline solid, but they are consistent with the presence of either high-spin Fe(II) or Fe(III).

The spectroscopic properties of $\{(py)_2Fe(OEPO)\}$ have received several interpretations. The complex is EPR silent at room temperature in pyridine solution, but it shows an axial spectrum with $g = 2.31$ and 1.75 when frozen at 77 K.[10] In pyridine solution, it has a magnetic moment of 2.4 μ_B at 23 °C.[10] The pattern of resonances in the ^{1}H NMR spectrum of this complex, which has two meso resonances in the upfield region and methylene resonances that exhibit both upfield and downfield hyperfine shifts, is unusual.[1,8,10,11] This pattern has suggested to some workers that there is a significant contribution from a ligand-based radical with the iron in a low-spin ($S = 0$) state.[10,11] The non-Curie behavior observed in the variable-temperature ^{1}H NMR spectrum[10] indicates that there may be temperature-dependent changes occurring either in the electronic distribution or in the spin state. The ^{1}H NMR spectrum of this complex has also been interpreted in terms of a low-spin $(d_{xz}d_{yz})^4(d_{xy})^1$ ground state.[12] However, this latter interpretation is at odds with the results of the crystallographic study at 143 K on the isolated complex.[9]

A number of complexes related to $\{(py)_2Fe(OEPO)\}$ but differing in axial ligation have been reported. Morishima and co-workers have examined the ^{1}H NMR spectra of a series of complexes with substituted pyridines and imidazoles as axial ligands,[11] while Makuoka and Itano have used tosylmethylisocyanide as an axial ligand.[13] Additionally, $[(NC)_2Fe(OEPO)]^{2-}$ has been observed during the coupled oxidation of Fe^{II}(OEP) in the presence of cyanide ion rather than pyridine.[14] Here, we examine the structural and spectroscopic properties of two complexes with either *N*-methylimidazole (1-MeIm) or 2,6-xylylisocyanide (2,6-xylylNC) as the axial ligands. Changing the axial ligand is shown to alter the electronic distribution between the metal and the porphyrin.

Results

Preparation of Compounds. Samples of $(1\text{-MeIm})_2Fe^{III}$-(OEPO) and $(2,6\text{-xylylNC})_2Fe^{II}(OEPO^{\bullet})$ were prepared by addition of an excess of the appropriate axial ligand to a slurry of $\{Fe^{III}(OEPO)\}_2$ in chloroform under anaerobic conditions as shown in Scheme 3. During the process, $\{Fe^{III}(OEPO)\}_2$, which is only slightly soluble, dissolves. The products were isolated as deep red or nearly black crystals by slowly diffusing *n*-hexane into the mixture after it was filtered. These six-coordinate adducts are stable in the solid state as long as they are protected from atmospheric dioxygen. In dioxygen-free solution in the absence of excess axial ligand, the products gradually lose their axial ligands, and $\{Fe^{III}(OEPO)\}_2$ precipitates from solution. In the presence of air, both complexes react rapidly to form the corresponding verdohemes.

Figure 1 compares the UV/vis spectra of the two new compounds. To minimize the effects of axial ligand dissociation, the spectra were run in the presence of added 1-MeIm or 2,6-xylylNC. Despite the similarity in synthesis and composition, the two spectra are notably different. The spectrum of $(1\text{-MeIm})_2Fe^{III}$(OEPO) shows an intense peak at 394 nm and broad absorption in the Soret region. In contrast, the spectrum of $(2,6\text{-xylylNC})_2Fe^{II}(OEPO^{\bullet})$ shows a gradual increase in the absorbance throughout the region and sharper Soret bands. In addition, $(2,6\text{-xylylNC})_2Fe^{II}(OEPO^{\bullet})$ shows an absorbance at 830 nm which is not shown in Figure 1. These variations in the spectra of the two complexes are indicative of differences in their electronic structures. Similar UV/vis spectra were reported by Masuoka and Itano for $(py)_2Fe^{III}$(OEPO) and $(\text{tosylmethylisocyanide})_2Fe^{III}$(OEPO).[13]

Magnetic Susceptibility Studies. The magnetic susceptibilities of $(1\text{-MeIm})_2Fe^{III}$(OEPO) and $(2,6\text{-xylylNC})_2Fe^{II}(OEPO^{\bullet})$ as crystalline solids have been determined as a function of temperature. Figure 2 shows a graph of the effective magnetic moment of the two complexes plotted versus the temperature. For $(2,6\text{-xylylNC})_2Fe^{II}(OEPO^{\bullet})$, the magnetic moment is constant and consistent with the presence of a complex with an $S = {}^1/_2$ spin state. For $(1\text{-MeIm})_2Fe^{III}$(OEPO), the magnetic moment drops from 4.8 μ_B at room temperature to 1.8 μ_B at 100 K and remains at that value upon further cooling. The magnetic behavior is indicative of a smooth spin-state change from an $S = {}^1/_2$ state at temperatures below 100 K to an $S = {}^5/_2$ or spin-admixed ${}^3/_2$,${}^5/_2$ state at high temperatures (near room temperature).

(8) Kalish, H. R.; Latos-Grażyński, L.; Balch, A. L. *J. Am. Chem. Soc.* **2000**, *122*, 12478.
(9) Balch, A. L.; Koerner, R.; Latos-Grażyński, L.; Noll, B. C. *J. Am. Chem. Soc.* **1996**, *118*, 2760.
(10) Morishima, I.; Fujii, H.; Shiro, Y. *J. Am. Chem. Soc.* **1986**, *108*, 3858.
(11) Morishima, I.; Fujii, H.; Shiro, Y.; Sano, S. *Inorg. Chem.* **1995**, *34*, 1528.
(12) Walker, F. A. *Coord. Chem. Rev.* **1999**, *186*, 471.
(13) Masuoka, N.; Itano, H. A. *Biochemistry* **1987**, *26*, 3672.
(14) Balch, A. L.; Koerner, R.; Latos-Grażyński, L.; Lewis, J. E.; St. Claire, T. N.; Zovinka, E. P. *Inorg. Chem.* **1997**, *36*, 3892.

Scheme 3

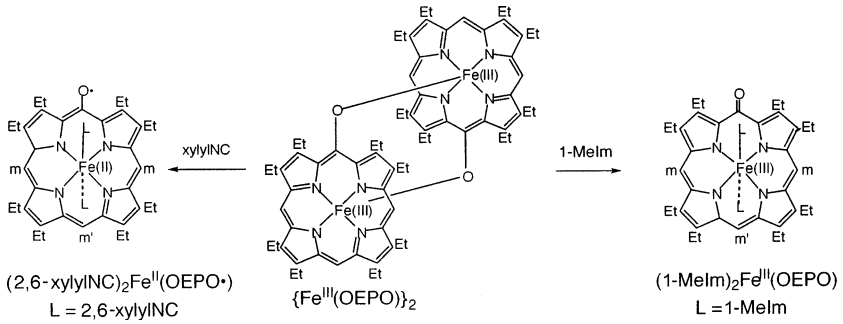

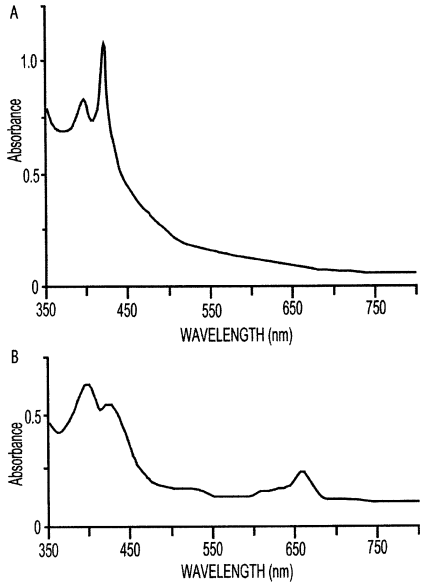

Figure 1. The UV/vis spectra recorded under dioxygen-free conditions of (A) $(2,6\text{-xyllNC})_2Fe^{II}(OEPO^{\bullet})$ and (B) $(1\text{-MeIm})_2Fe^{III}(OEPO)$ in dichloromethane solution containing 1% 2,6-xylylNC or 1-MeIm, respectively, at 298 K. For $(1\text{-MeIm})_2Fe^{III}(OEPO)$ (λ_{max}, nm (ϵ, M^{-1} cm^{-1})): 394 (2.8×10^4), 432 (1.9×10^4), 530 (6.2×10^3), 612 (5.4×10^3, sh), 662 (1.2×10^4). For $(2,6\text{-xyllNC})_2Fe^{II}(OEPO^{\bullet})$ (λ_{max}, nm (ϵ, M^{-1} cm^{-1})): 400 (3.3×10^4), 422 (5.5×10^4), 540 (6.5×10^3), 830 (9.8×10^3).

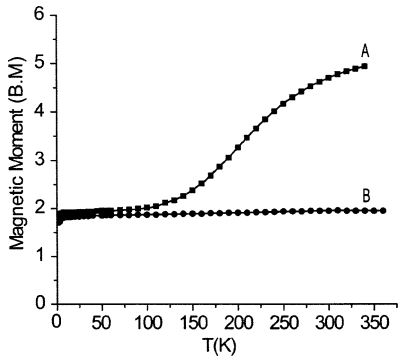

Figure 2. The magnetic moment of crystalline samples of (A) $(1\text{-MeIm})_2Fe^{III}(OEPO)$ and (B) $(2,6\text{-xylylNC})_2Fe^{II}(OEPO^{\bullet})$ as a function of temperature.

Single-Crystal X-ray Diffraction of $(1\text{-MeIm})_2Fe^{III}(OEPO)$ at 90 K. The complex crystallizes in the triclinic space group $P\bar{1}$. The asymmetric unit consists of one-half of the entire molecule with the iron atom located at a center of symmetry. Selected interatomic distances and angles are given in Table 1, while crystal data are given in Table 2. Figure 3 shows the structure of the complex. The iron is, as expected, six-coordinate. Because the complex is centrosymmetric, the planes of the two axial ligands are rigorously parallel to one another. The plane of the 1-MeIm ligand is canted by 13.5° away from the direction of the Fe−N1 bond.

The oxygen atom is disordered over the four meso positions. Such disorder is common in meso-substituted derivatives of octaethylporphyrin. For example, $\{(py)_2Fe(OEPO)\}$ shows similar disorder,[9] as do $ClFe^{III}$(*meso*-NC-OEP)[15] and $Zn^{II}(OEPO^{\bullet})$.[16] The major site, which is the one shown in Figure 3, has

Table 1. Selected Bond Lengths (Å) and Bond Angles (deg) for $(1\text{-MeIm})_2Fe^{III}(OEPO)$ and $(2,6\text{-xylylNC})_2Fe^{II}((OEPO^{\bullet})$

	$(1\text{-MeIm})_2Fe^{III}(OEPO)$	$(1\text{-MeIm})_2Fe^{III}(OEPO)$	$(1\text{-MeIm})_2Fe^{III}(OEPO)$	$(2,6\text{-xylylNC})_2Fe^{II}(OEPO^{\bullet})$
temp, K	296(2)	129(2)	90(2)	90(2)
		Bond Lengths		
Fe−N1	2.041(3)	2.017(3)	2.0163(15)	2.0200(12)
Fe−N2	2.025(3)	2.002(3)	2.0017(15)	2.0139(12)
Fe−N3 or C19	2.199(4)	1.994(3)	1.9904(16)	1.8908(15)
C1−O5	1.25(3)	1.246(19)	1.268(10)	1.230(13)
C10−O2	1.28(2)	1.28(3)	1.278(9)	1.266(3)
		Bond Angles		
N1−Fe−N2	89.54(13)	89.50(11)	89.61(6)	90.77(5)
N1−Fe−N3 or C19	91.27(13)	91.09(11)	90.97(6)	90.19(5)
N2−Fe−N3 or C19	88.75(13)	88.96(11)	88.99(6)	85.74(5)

Table 2. Crystal Data and Data Collection Parameters

	$(1\text{-MeIm})_2Fe^{III}(OEPO)$	$(1\text{-MeIm})_2Fe^{III}(OEPO)$	$(1\text{-MeIm})_2Fe^{III}(OEPO)$	$(2,6\text{-xylylNC})_2Fe^{II}(OEPO^{\bullet})$
T, K	296(2)	129(2)	90(2)	90(2)
formula	$C_{44}H_{53}FeN_8O$	$C_{44}H_{53}FeN_8O$	$C_{44}H_{53}FeN_8O$	$C_{54}H_{59}FeN_6O$
formula weight	765.79	765.79	765.79	863.92
color and habit	red plate	red plate	red plate	dark block
crystal system	triclinic	triclinic	triclinic	orthorhombic
space group	$P\bar{1}$	$P\bar{1}$	$P\bar{1}$	*Pccn*
a, Å	9.6554(9)	9.5027(6)	9.4992(14)	20.079(2)
b, Å	10.6473(10)	10.4786(7)	10.4689(15)	21.373(2)
c, Å	10.7277(12)	10.5971(8)	10.5854(16)	10.5266(11)
α, deg	98.262(8)	98.151(6)	98.140(3)	90
β, deg	90.685(8)	90.643(6)	90.682(3)	90
γ, deg	115.702(7)	115.179(5)	115.099(3)	90
V, Å^3	980.00(17)	942.28(11)	940.6(2)	4517.5(8)
radiation (λ, Å)	Cu Kα (1.54178)	Cu Kα (1.54178)	Mo Kα (0.71073)	Mo Kα (0.71073)
Z	1	1	1	4
d_{calcd}, g•cm^{-3}	1.298	1.350	1.352	1.270
μ, mm^{-1}	3.437	3.574	0.448	0.381
range of transm. factors	0.42−0.77	0.41−0.76	0.88−0.97	0.93−0.98
no. of unique data	2555	2457	3440	4915
no. of restraints	0	0	0	0
no. of params. refined	265	265	265	290
R1[a]	0.058	0.052	0.035	0.036
wR2[b]	0.166	0.135	0.087	0.092

[a] For data with $I > 2\sigma I$. $R1 = (\sum||F_o| - |F_c||)/(\sum|F_o|)$. [b] For all data. $wR2 = \sqrt{(\sum[w(F_o^2-F_c^2)^2])/(\sum[w(F_o^2)^2])}$.

(15) Kalish, H.; Camp, J. E.; Stępień, M.; Latos-Grażyński, L.; Olmstead, M. M.; Balch, A. L. *Inorg. Chem.* **2002**, *41*, 989.

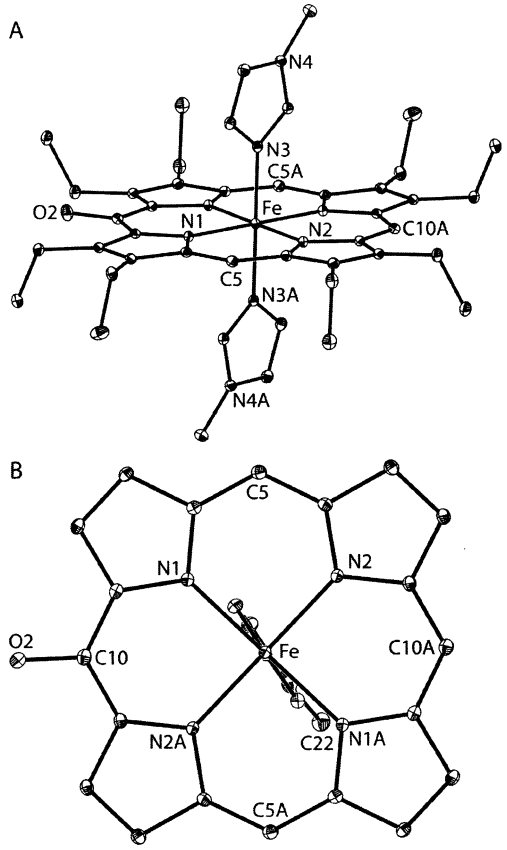

Figure 3. A perspective view of (1-MeIm)$_2$Fe^{III}(OEPO) showing 30% thermal contours from the data taken at 90 K. Only one of the four sites for the oxygen atom is shown. This site has a fractional occupancy of 0.28.

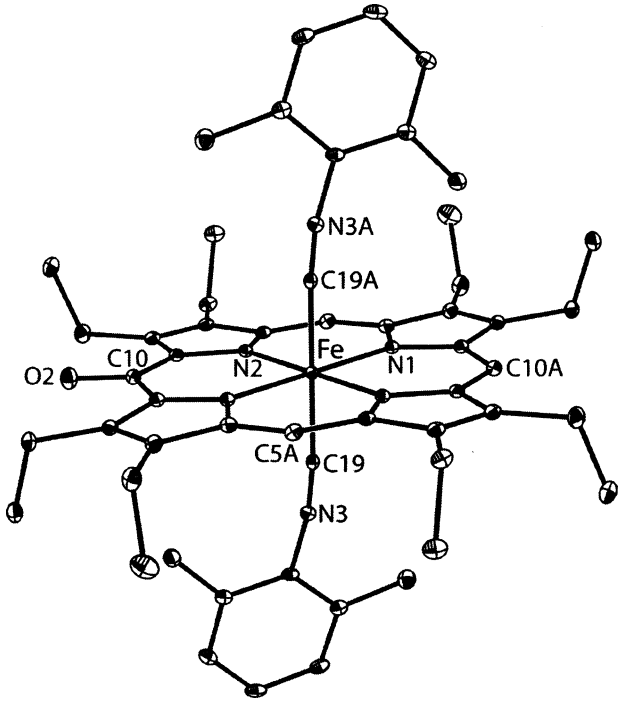

Figure 4. A perspective view of (2,6-xylylNC)$_2$Fe^{II}(OEPO$^{\bullet}$) showing 30% thermal contours. Only one of the four sites for the oxygen atom is shown. This site has a fractional occupancy of 0.40.

0.28 occupancy. Because the complex is centrosymmetric, there is a second oxygen atom bound to the opposite side of the porphyrin with 0.28 occupancy as well. The C−O distance at this site is 1.268(10) Å, a distance that is indicative of significant C−O double bond character. The other two meso positions also bear oxygen atoms with fractional occupancies of 0.22 at each site. At this position, the C−O distance is 1.278(9) Å, which is similar to the distance at the major site.

The Fe−N1 and Fe−N2 distances, which are the in-plane distances to the porphyrin nitrogen atoms, are 2.0163(15) and 2.0017(15) Å, respectively. The axial Fe−N3 distance is very slightly shorter, 1.9904(16) Å.

The structural parameters for (1-MeIm)$_2$Fe^{III}(OEPO) are quite similar to those of a number of six-coordinate, $S = {}^1/_2$ iron(III) porphyrins that have parallel or nearly parallel axial imidazole ligands. For example, [(1-MeIm)$_2$Fe^{III}(TPP)]ClO$_4$ (TPP is the dianion of tetra-(phenyl)porphyrin) has a nearly parallel arrangement of the two axial imidazole ligands.[17] From the structure obtained at 298 K, it has in-plane Fe−N distances of 1.969(3), 1.988(3), 1.969(3), and 1.993(3) Å, while the axial Fe−N distances are 1.978(3) and 1.970(3) Å. Similarly, the isomer of [(5-MeIm)$_2$Fe^{III}(TMP)]ClO$_4$ (TMP is the dianion of tetra-(mesityl)porphyrin), which has the two axial ligands in a nearly parallel orientation, has in-plane Fe−N(porphyrin) distances of 1.986(5) and 1.978(5) Å in one of the crystallographically independent molecules and Fe−N(porphyrin) distances of 1.981(5) and 1.974(5) Å in the other from data acquired at 127 K.[18] The axial Fe−N(imidazole) distances in both molecules are 1.985(5) Å. In [(1-MeIm)$_2$Fe^{III}(TPP)]ClO$_4$, the planes of the axial ligands are displaced by 22° and 32° from the nearest Fe−N bonds.[16] In [(5-MeIm)$_2$Fe^{III}(TMP)]ClO$_4$, the planes of the axial ligands are offset from the nearest Fe−N bond by 10° and 20° in one molecule and by 12° and 14° in the other.[17]

The porphyrin macrocycle in (1-MeIm)$_2$Fe^{III}(OEPO) is nearly planar with the largest out-of-plane displacement of any of the core atoms being only 0.035 Å.

Comparison of the Crystal Structure of (1-MeIm)$_2$Fe^{III}(OEPO) at Variable Temperatures. The structure of (1-MeIm)$_2$Fe^{III}(OEPO) has also been determined at 298 and 129 K. The space group does not change at these temperatures, but the volume of the unit cell expands by 4.2% upon warming. This change results in gradual lengthening of the bonds. As seen in Table 1, the effect of warming is most pronounced in the length of the axial Fe−N(1-MeIm) bond. This bond expands from 1.9904(16) Å at 90 K to 2.199(4) Å at 296 K. In contrast, the in-plane Fe−N(porphyrin) distances expand only slightly from 2.0163(15) and 2.0017(15) Å at 90 K to 2.041(3) and 2.025(3) Å at 296 K. The elongation of the axial Fe−N distances is indicative of the presence of a high-spin compound at higher temperatures.

Single-Crystal X-ray Diffraction of (2,6-xylylNC)$_2$Fe^{II}(OEPO$^{\bullet}$). The crystal structure of (2,6-xylylNC)$_2$Fe^{II}(OEPO$^{\bullet}$) was determined at 90 K. The complex crystallizes in the orthorhombic space group *Pccn* with the iron atom again located at a center of symmetry. Figure 4 shows a drawing of the entire six-coordinate complex. There is disorder in the position of the oxygen atom. The site shown in Figure 4 has a fractional

(16) Balch, A. L.; Noll, B. C.; Zovinka, E. P. *J. Am. Chem. Soc*. **1991**, *114*, 3380.
(17) Higgins, T. B.; Safo, M. K.; Scheidt, W. R. *Inorg. Chim. Acta* **1990**, *178*, 261.
(18) Munro, O. Q.; Serth-Guzzo, J. A.; Turowska-Tyrk, I.; Mohanrao, K.; Shokhireva, T. Kh.; Walker, F. A.; Debrunner, P. G.; Scheidt, W. R. *J. Am. Chem Soc*. **1999**, *121*, 11144.

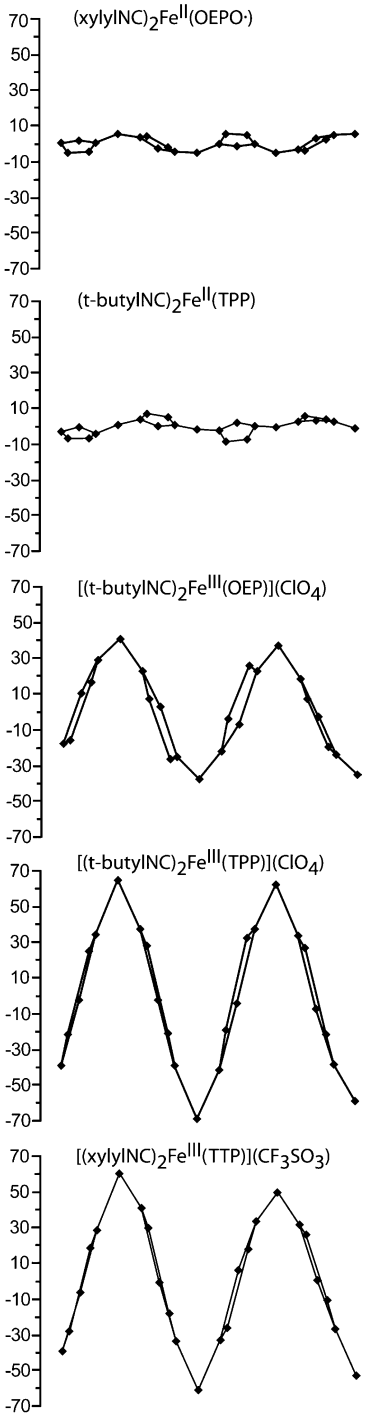

Figure 5. Diagrams comparing the out-of-plane displacements in the units of 0.01 Å of the porphyrin core atoms from the mean plane of the porphyrin for (2,6-xylylNC)$_2$Fe^{II}(OEPO$^{\bullet}$), (*tert*-butylNC)$_2$Fe^{II}(TPP) (data from ref 19), (*tert*-butylNC)$_2$Fe^{III}(OEP)](ClO$_4$) (data from ref 20), (*tert*-butylNC)$_2$Fe^{III}-(TPP)](ClO$_4$) (data from ref 20), and (2,6-xylylNC)$_2$Fe^{III}(tetrakis(*p*-tolyl)-porphyrin)](CF$_3$SO$_3$) (data from ref 21).

occupancy of 0.40. Because of the center of symmetry, there is an equally populated site for the oxygen atom at the opposite side of the ring. Additionally, the oxygen atom resides at the other two meso carbons with site occupancies of 0.10. As noted above, this sort of disorder is frequent in the solid-state structures of complexes of octaethylporphyrin in which there is a relatively small group occupying one of the meso positions.

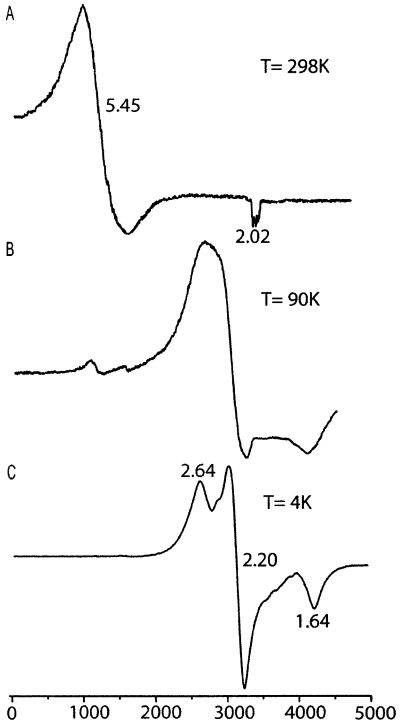

Figure 6. The EPR spectrum of a polycrystalline sample of (1-MeIm)$_2$Fe^{III}-(OEPO) at (A) 298, (B) 90, and (C) 4.2 K.

The Fe−N bond distances (2.0200(12) and 2.0139(12) Å) and the Fe−C bond distance (1.8908(15) Å) are similar to those in the iron(II) complex, (*tert*-butylNC)$_2$Fe^{II}(TPP), which has Fe−N distances in the range 2.000(2)−2.010(2) Å and Fe−C distances of 1.900(3) and 1.901(3) Å.[19] However, iron(III) porphyrins with two axial isocyanide ligands have very similar metal−ligand distances. Thus, the Fe−N distances in (*tert*-butylNC)$_2$Fe^{III}(OEP)](ClO$_4$) fall in the range 1.952(3)−1.994(3) Å and the Fe−C distances are 1.925 and 1.929 Å.[20] In (*tert*-butylNC)$_2$Fe^{III}(TPP)](ClO$_4$), the Fe−N distances range from 1.918(16) to 1.962(16) Å and the Fe−C distances are 1.902(18) and 1.93(2) Å,[20] while in (2,6-xylylNC)$_2$Fe^{III}(tetrakis(*p*-tolyl)-porphyrin)](CF$_3$SO$_3$) the Fe−N distances vary from 1.937(7) to 1.974(7) Å and the Fe−C distances are 1.92(2) and 1.95(1) Å.[21]

However, the porphyrins in these iron(III) complexes suffer a greater distortion from planarity than is seen for either (2,6-xylylNC)$_2$Fe^{II}(OEPO$^{\bullet}$) or the iron(II) complex, (*tert*-butylNC)$_2$Fe^{II}-(TPP). Relevant data are shown in Figure 5, where the out-of-plane displacements of the porphyrin core atoms are plotted.

While the C−Fe−C portion of (2,6-xylylNC)$_2$Fe^{II}(OEPO$^{\bullet}$) is strictly linear because of the crystallographic symmetry, the Fe−C19−N3 angle (173.17(13)°) is bent as is the neighboring C19−N3−C20 angle (169.09(14)°).

EPR Spectra. The X-band EPR spectrum of a polycrystalline sample of (1-MeIm)$_2$Fe^{III}(OEPO) shows a marked temperature dependence as shown in Figure 6. The *g* values recorded at 4 K (2.64, 2.20, and 1.64) are similar to those of other related low-spin Fe(III) porphyrins with axial ligands in a parallel orientation. For example, (5-MeIm)$_2$Fe^{III}(TMP)](ClO$_4$) has $g_1 = 2.69$, $g_2 = 2.34-2.43$, $g_3 = 1.75$;[18] and (N-MeIm)$_2$Fe^{III}(TPP)]-(ClO$_4$) has $g_1 = 2.866$, $g_2 = 2.276$, $g_3 = 1.535$.[17] On warming, the EPR spectra change as seen in Figure 6. At 298 K, an axial spectrum with $g_\perp = 5.45$ and $g_{||} = 2.02$ is observed.

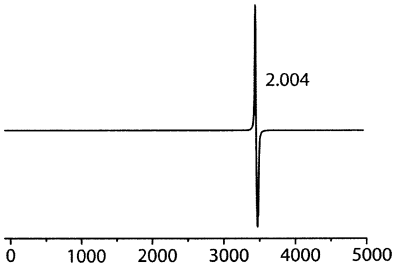

Figure 7. The EPR spectrum of a polycrystalline sample of (2,6-xylylNC)$_2$Fe^{II}(OEPO$^{\bullet}$) at 298 K.

In contrast to the temperature-dependent behavior of (1-MeIm)$_2$Fe^{III}(OEPO), the EPR spectrum of (2,6-xylylNC)$_2$Fe^{II}-(OEPO$^{\bullet}$) consists of a narrow single line that is not affected by changes in temperature. Figure 7 shows the spectrum obtained at 298 K with an isotropic signal with $g = 2.004$ and a peak-to-peak separation of 24.4 G.

For comparison with the EPR spectra expected for low-spin iron(III) complexes, axial EPR spectra are seen for both [(PhNC)$_2$Fe^{III}(TPP)]$^+$ with $g_\perp = 2.20$, $g_\parallel = 1.95$ and for [(PhNC)$_2$Fe^{III}-(OEP)]$^+$ with $g_\perp = 2.25$, $g_\parallel = 1.91$.[22] These complexes have the $(d_{xz},d_{yz})^4(d_{xy})^1$ electronic configuration with the unpaired electron in an iron d_{xy} orbital.

Discussion

The results presented here show that the nature of the axial ligand can alter the distribution of electrons between the metal and the porphyrin in complexes of the type {L$_2$Fe(OEPO)}. The two complexes reported here serve as particularly clear examples of two distinct distributions. Thus, for (1-MeIm)$_2$Fe^{III}(OEPO), the tetrapyrrole macrocycle is present in the trianionic oxophlorin form and the metal is Fe(III). With (2,6-xylylNC)$_2$Fe^{II}-(OEPO$^{\bullet}$), the ligand is present as a dianionic radical and the metal is low-spin Fe(II). In the latter case, π-back-bonding to the acceptor isocyanide ligands contributes to stabilization of the low-spin Fe(II) state. Several other examples of complexes containing the radical ligand (OEPO$^{\bullet}$) have been reported. Oxidation of (py)Zn^{II}(OEPOH) and (py)Ni^{II}(OEPOH) with either dioxygen or di-iodine produces the stable free radicals, (py)Zn^{II}(OEPO$^{\bullet}$) and (py)Ni^{II}(OEPO$^{\bullet}$).[16,23] These radicals produce sharp, unstructured EPR spectra at $g = 2.00$. Additionally, oxidation of {Fe^{III}(OEPO)}$_2$ with bromine produces the highly oxidized complex BrFe^{III}(OEPO$^{\bullet}$), which contains two paramagnetic centers, the ligand radical, and the Fe(III) ion.[24]

The observation of an isotropic EPR signal for (2,6-xylylNC)$_2$Fe^{II}(OEPO$^{\bullet}$) with $g = 2.004$ and a peak-to-peak separation of 24.4 G provides a well-characterized model for a previously detected intermediate formed during oxidation of the meso-hydroxylated heme bound to heme oxygenase. The hydroxylated heme/heme oxygenase complex displays an EPR signal with resonances at $g = 6.07$ and 5.71 due to the high-spin iron(III) heme along with a readily saturated, free radical signal at $g = 2.008$[25] or 2.004.[26] The intensity of the free radical signal is enhanced at the expense of the resonances of the high-spin form at $g = 6.07$ and 5.71 when carbon monoxide (a product of heme oxygenase activity) is added to the sample. These EPR observations have been interpreted to indicate that carbon monoxide coordinates the iron in the hydroxylated heme/heme oxygenase complex and creates a form in which the iron(II)-heme radical resonance structure dominates the electronic structure.[25,26] Our results demonstrate that appropriate axial ligands can stabilize the iron(II)-heme radical structure and produce a free-radical like EPR resonance near $g = 2$. Thus, in (2,6-xylylNC)$_2$Fe^{II}(OEPO$^{\bullet}$), the two π-accepting axial isocyanide ligands stabilize the low-spin Fe(II) state of the metal and the radical form of the macrocycle. However, in regard to heme ligation, carbon monoxide and isocyanides are rather different ligands. Thus, as the information used to create Figure 5 shows, isocyanides readily form complexes with two axial ligands with both iron(II) and iron(III). On the other hand, carbon monoxide binds only to iron(II) hemes. Moreover, binding of two axial carbon monoxide ligands occurs only under forcing conditions.[27] Consequently, further work is needed to identify the nature of the complex responsible for the free radical signal at $g = 2.008$ or 2.004, for example, by examining the reactivity of carbon monoxide itself with meso-hydroxylated hemes such as {(py)$_2$Fe-(OEPO)} and isolating the products that are formed.

A related case where axial ligation alters the electronic distribution between metal and tetrapyrrole ligand is found in the octaethylbilindione complexes of cobalt shown in Scheme 3.[28] Here, a change in the number of axial ligands is the key factor in determining the electronic distribution. The EPR spectrum of [Co^{II}(OEBOx)]$^+$ shows a characteristic Co(II) spectrum with $g_{x,y} = 2.29$, $g_z = 2.013$, $A_x = 16 \times 10^{-4}$ cm^{-1}, $A_y = 35 \times 10^{-4}$ cm^{-1}, $A_z = 89.3 \times 10^{-4}$ cm^{-1}. Addition of pyridine produces [Co^{II}(OEBO$^{\bullet}$)]$^+$, which shows a slightly asymmetric resonance with $g_{x,y} = 2.29$, $g_z = 2.013$, and no cobalt hyperfine coupling. These spectral features are indicative of the presence of a largely ligand-based free radical in the six-coordinate complex.

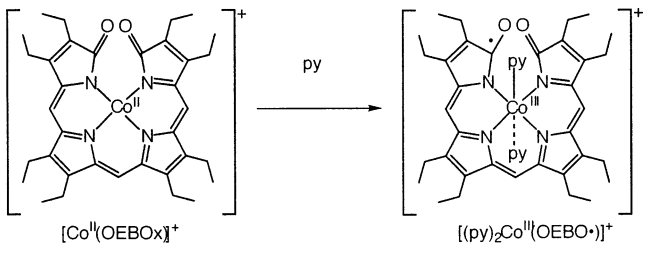

For (1-MeIm)$_2$Fe^{III}(OEPO), the data compiled here indicate that the metal is present in the iron(III) oxidation state. However, the iron(III) spin state of this complex varies with temperature. At low temperatures, it exists in the low-spin ($S = {}^1/_2$) state that is common for most six-coordinate Fe(III) hemes with two

(19) Jameson, G. B.; Ibers, J. A. *Inorg. Chem.* **1979**, *18*, 1200.
(20) Walker, F. A.; Nasri, H.; Turowska-Tyrk, I.; Mohanrao, K.; Watson, C. T.; Shokhirev, N. V.; Debrunner, P. G.; Scheidt, W. R. *J. Am. Chem. Soc.* **1996**, *118*, 12109.
(21) Simonneaux, G.; Schünemann, V.; Morice, C.; Carel, L.; Toupet, L.; Winkler, H.; Trautwein, A. X.; Walker, F. A. *J. Am. Chem. Soc.* **2000**, *122*, 4366.
(22) Astahkin, A. V.; Raitsimring, A. M.; Kennedy, A. R.; Shokhireva, T. Kh.; Walker, F. A. *J. Phys. Chem. A* **2002**, *106*, 74.
(23) Balch, A. L.; Noll, B. C.; Phillips, S. L.; Reid, S. M.; Zovinka, E. P. *Inorg. Chem.* **1993**, *32*, 4730.
(24) Balch, A. L.; Latos-Grażyński, L.; Noll, B. C.; Szterenberg, L.; Zovinka, E. P. *J. Am. Chem. Soc.* **1993**, *115*, 11846.
(25) Liu, Y.; Moënne-Loccoz, P.; Loehr, T. M.; Ortiz de Montellano, P. R. *J. Biol. Chem.* **1997**, *272*, 6909.
(26) Sakamoto, H.; Omata, Y.; Palmer, G.; Noguchi, M. *J. Biol. Chem.* **1999**, *274*, 18196.
(27) Wayland, B. B.; Mehne, L. F.; Swartz, J. *J. Am. Chem. Soc.* **1978**, *100*, 2379.
(28) Attar, S.; Ozarowski, A.; Van Calcar, P. M.; Winkler, K.; Balch, A. L. *Chem. Commun.* **1997**, 1115.
(29) Benda, R.; Schüneman, V.; Trautwein, A. X.; Cai, S.; Polam, J. R.; Watson, C. T.; Shokhireva, T. Kh.; Walker, F. A. *J. Biol. Inorg. Chem.* **2003**, *8*, 787.

heterocyclic amines as axial ligands. For such low-spin Fe(III) hemes, the orientations of the planes of axial ligands affect the spectroscopic features and the electronic structures of the complexes.[12,18,29] Type I complexes have a $(d_{xy})^2(d_{xz},d_{yz})^3$ electronic configuration and axial ligands aligned perpendicular to each other. Such complexes are characterized by EPR spectra of the "large g_{max}" class. Type II complexes also have a $(d_{xy})^2(d_{xz},d_{yz})^3$ electronic configuration but have the axial ligands aligned parallel to one another. Type II complexes have rhombic EPR spectra of the sort seen here for $(1\text{-MeIm})_2Fe^{III}(OEPO)$ at low temperature. Type III complexes have the less common $(d_{xz},d_{yz})^4(d_{xy})^1$ electronic ground state and display axial EPR spectra with $g_\perp \approx 2.6$.

The temperature-dependent changes seen in the crystal structure, the magnetic moment, and the EPR spectra of $(1\text{-MeIm})_2Fe^{III}(OEPO)$ are indicative of a change in spin state, while the electronic distribution between the metal and the ligand remains constant. The data suggest that the complex exists in the high-spin ($S = {}^5/_2$) or a spin-admixed ($S = {}^3/_2,{}^5/_2$) state at high temperatures shown in Figure 2. The elongation of the axial Fe−N bond on warming is consistent with the population of either an admixed $S = {}^3/_2,{}^5/_2$ or an $S = {}^5/_2$ state at higher temperatures. For comparison, six-coordinate $((CN)_3C)Fe^{III}$-(TPP), which has been assigned as an intermediate spin ($S = {}^3/_2$) complex, has an axial Fe−N distance of 2.317(3) Å and in-plane Fe−N(porphyrin) distances of 1.995(3), 1.996(3), 1.999(3), and 1.991(3) Å.[30] The EPR spectrum of $((CN)_3C)$-Fe^{III}(TPP) at 78 K is axial with $g_\perp = 5.26$ and $g_{||} = 2.00$. For $[(1\text{-Cl-py})_2Fe^{III}(OEP)](ClO_4)$, the resolved axial Fe−N distance is 2.316 Å in the $S = {}^5/_2$ state (vide infra).[31]

Cases of reversible spin crossover are known for several six-coordinate iron(III) porphyrins with two heterocyclic amine ligands. For example, $[(2\text{-MeIm})_2Fe^{III}(OEP)](ClO_4)$[32,33] undergoes spin crossover from an $S = {}^1/_2$ state at low temperature to an admixed state at high temperature with predominant $S = {}^5/_2$ character. The axial ligands are in a parallel orientation, and the axial Fe−N bond undergoes significant expansion on warming. The behavior of $[(1\text{-Cl-py})_2Fe^{III}(OEP)](ClO_4)$ is more complex. As a solid, $[(1\text{-Cl-py})_2Fe^{III}(OEP)](ClO_4)$ forms two polymorphs, a triclinic one that undergoes thermal spin crossover[26,34] and a monoclinic form that contains a quantum-admixed ($S = {}^3/_2,{}^5/_2$) state.[35] The highly distorted complex, $[(py)_2Fe^{III}$(octaethyltetraphenylporphyrin)$](ClO_4)$, also undergoes spin crossover between an $S = {}^1/_2$ state at low temperature and an $S = {}^3/_2$ state at 298 K.[36,37] Because $(1\text{-MeIm})_2Fe^{III}(OEPO)$ undergoes a spin state change but contains an axial ligand that usually produces a low-spin iron(III) porphyrin, it is likely that the ligand field strength of the trianionic oxophlorin ligand is larger than that of a typical dianionic porphyrin. Consequently, the greater in-plane ligand field of the oxophlorin acts to reduce the energy gaps between the d orbitals and promotes spin crossover in $(1\text{-MeIm})_2Fe^{III}(OEPO)$.

Experimental Section

Materials. Iron(III)octaethylporphyrin chloride was purchased from Mid Century. Samples of $\{Fe^{III}(OEPO)\}_2$ were prepared by an established route.[38]

Preparation of $(1\text{-MeIm})_2Fe^{III}(OEPO)$. Under an atmosphere of purified dinitrogen, 0.50 mL (6.3 mmol) of 1-methyl imidazole was added to a suspension of 50 mg (0.043 mmol) of $\{Fe^{III}(OEPO)\}_2$ in 10 mL of dioxygen-free chloroform. The mixture was stirred for 5 min to form a deep green solution. This solution was filtered to remove any solid residue, and then the volume of the solution was reduced to one-half under reduced pressure. Dioxygen-free *n*-hexane was carefully layered over the solution in a dinitrogen-filled glovebox. On standing for 4 or 5 days, dark red crystals of the products formed. The crystals were collected by filtration, washed with *n*-hexane, and vacuum-dried: yield 33 mg (0.042 mmol), 50%. UV/vis spectra (under N_2 atmosphere) in dichloromethane with 1% 1-MeIM added to retard dissociation back to $\{Fe^{III}(OEPO)\}_2$ (λ_{max}, nm (ϵ, M^{-1} cm^{-1})): 394 (2.8×10^4), 432 (1.9×10^4), 530 (6.2×10^3), 612 (5.4×10^3, sh), 662 (1.2×10^4).

Preparation of $(2,6\text{-xylylNC})_2Fe^{II}(OEPO^\bullet)$. Under an atmosphere of purified dinitrogen, 1.0 g of 2,6-xylylNC (7.6 mmol) was added to a suspension of 50 mg (0.043 mmol) of $\{Fe^{III}(OEPO)\}_2$ in 10 mL of dioxygen-free chloroform. The mixture was stirred for 5 min to form a dark brown solution. This solution was filtered to remove any solid residue, and then the volume of the solution was reduced to one-half under reduced pressure. Dioxygen-free *n*-hexane was carefully layered over the solution in a dinitrogen-filled glovebox. On standing for 4 or 5 days, dark red crystals of the product formed. The crystals were collected by filtration, washed with *n*-hexane, and vacuum-dried: yield 44 mg (0.051 mmol), 59%. UV/vis spectra (under N_2 atmosphere) in dichloromethane with 1% 2,6-xylylNC (λ_{max}, nm (ϵ, M^{-1} cm^{-1})): 400 (3.3×10^4), 422 (5.5×10^4), 830 (9.8×10^3).

X-ray Data Collection. Crystals of the two complexes were obtained directly from the preparations as described above. The crystals were coated with a light hydrocarbon oil and mounted in the 90 K dinitrogen stream of a Bruker SMART 1000 diffractometer equipped with CRYO Industries low-temperature apparatus. Intensity data were collected using graphite-monochromated Mo Kα radiation. Crystal data are given in Table 2. Intensity data at 296 and 129 K were collected using Ni-filtered Cu Kα radiation (λ, 1.54178 Å) on a Siemens P4 rotating anode diffractometer equipped with a Siemens LT-2 low-temperature device.

Solution and Structure Refinement. Scattering factors and correction for anomalous dispersion were taken from a standard source.[39] An absorption correction was applied.[40] The solution of the structure was obtained by direct methods with SHELXS-97 and subsequent cycles of least-squares refinement on F^2 with SHELXL-97.

Instrumentation. The X-band EPR spectra were recorded on a Bruker ECS-106 instrument equipped with an Oxford Instruments variable-temperature liquid helium cryostat. The microwave frequency was measured by using a calibrated cavity resonator, and the magnetic field intensity was checked using solid DPPH as a standard. Magnetic susceptibility data were collected on a Quantum Design MPMS superconducting quantum interference device (SQUID) magnetometer with a 7-T superconducting magnet. The data were collected and

(30) Summerville, D. A.; Cohen, I. A.; Hatano, K.; Scheidt, W. R. *Inorg. Chem.* **1978**, *17*, 2906.
(31) Scheidt, W. R.; Geiger, D. K.; Haller, K. J. *J. Am. Chem. Soc*. **1982**, *104*, 495.
(32) Geiger, D. K.; Lee, Y. J.; Scheidt, W. R. *J. Am. Chem. Soc*. **1984**, *106*, 6339.
(33) Elkaim, E.; Tanaka, K.; Coppens, P.; Scheidt, W. R. *Acta Crystallogr.* **1987**, *B43*, 457.
(34) Gregson, A. K. *Inorg. Chem.* **1981**, *20*, 81.
(35) Scheidt, W. R.; Geiger, D. K.; Hayes, R. J.; Lang, G. *J. Am. Chem. Soc*. **1983**, *105*, 2524.
(36) Ikeue, T.; Ohgo, Y.; Yamaguchi, T.; Takahashi, M.; Takeda, M.; Nakamura, M. *Angew. Chem., Int. Ed.* **2001**, *40*, 2617.
(37) Ohgo, Y.; Ikeue, T.; Nakamura, M. *Inorg. Chem.* **2002**, *41*, 1698.
(38) Balch, A. L.; Koerner, R.; Latos-Grażyński, L.; Lewis, J. E.; St. Claire, T. N.; Zovinka, E. P. *Inorg. Chem.* **1997**, *36*, 3892.
(39) *International Tables for Crystallography*; Kluwer Academic Publishers: Dordrecht, The Netherlands, 1992.
(40) (a) SADABS 2.05: Sheldrick, G. M., University of Göttingen, Germany (SMART data). (b) XABS: Parkin, S.; Moezzi, B.; Hope, H. *J. Appl. Crystallogr*. **1995**, *28*, 53 (P4 data).

analyzed through the use of Design Magnetic Property Measurement System (MPMS) MultiVu software.

Acknowledgment. We thank the NIH (Grant GM-26226, A.L.B.) and the NSF (Grant OSTI 97-24412) for partial funding of the 500 MHz NMR spectrometer.

Supporting Information Available: Crystallographic details (CIF). This material is available free of charge via the Internet at http://pubs.acs.org.

JA0316014